Epigenetic silencing of HTATIP2 in glioblastoma enhances nuclear translocation of the DNA-repair protein MPG affecting treatment resistance

Monika Hegi (monika.hegi@chuv.ch)
Lausanne University Hospital and University of Lausanne https://orcid.org/0000-0003-0855-6495
Thi Tham Nguyen
Lausanne University Hospital and University of Lausanne
Premnath Rajakannu
Lausanne University Hospital and University of Lausanne
Minh Diêu Thanh Pham
Lausanne University Hospital and University of Lausanne
Leo Weman
Lausanne University Hospital and University of Lausanne
Alexander Jucht
Lausanne University Hospital and University of Lausanne
Michelle Buri
Lausanne University Hospital and University of Lausanne https://orcid.org/0000-0001-7261-0201
Kristof Van Dommelen
Lausanne University Hospital and University of Lausanne

Article

Keywords:

Posted Date: November 15th, 2022

DOI: https://doi.org/10.21203/rs.3.rs-2266918/v1

Abstract

DNA methylome analysis of glioblastoma (GBM) identified the HIV-1 Tat interactive protein 2 (*HTATIP2)* gene as aberrantly methylated and silenced. HTATIP2 is a negative regulator of importin β-mediated (KPNB1) cytoplasmic-nuclear translocation of proteins and its deregulation may alter the functionality of cancer relevant nuclear proteins. We propose N-Methylpurine-DNA Glycosylase (MPG), responsible for removing alkylated bases and initiating base excision repair (BER), as a potential GBM relevant candidate. Here we investigated the role of epigenetic silencing of *HTATIP2* on the subcellular localization of MPG, and MPG-mediated DNA repair.

Induction of *HTATIP2* expression in GBM cells lead to a significant shift of predominantly nuclear to cytoplasmic MPG, while depletion of endogenous levels of *HTATIP2* resulted in enhanced nuclear MPG localization. We observed exclusion of MPG from the area exhibiting co-localization of HTATIP2 and KPNB1 in proximity to the nuclear membrane, suggesting competition of HTATIP2 with MPG to bind to KPNB1. In accordance, pharmacologic inhibition of KPNB1 similarly induced cytoplasmic retention of MPG as HTATIP2 expression. Reduced nuclear MPG localization, induced by HTATIP2 expression or depletion of MPG, yielded less P-H2AX-positive cells upon treatment with an alkylating agent. This suggested reduced MPG-mediated formation of apurinic/apyrimidinic (AP) sites, leaving behind unrepaired DNA lesions, hence, reflecting a reduced capacity of BER in response to the alkylating agent.

Taken together, these results suggest that epigenetic silencing of *HTATIP2* may increase nuclear localization of MPG, thereby increasing the capacity of the tumor cells to repair treatment related lesions and eventually contributing to treatment resistance.

Introduction

Glioblastoma is one of the most aggressive malignant brain tumors in adults, notorious for treatment resistance with a median survival of only 15 months. The standard of care relies on genotoxic treatments combining radiotherapy with alkylating agents [1, 2]. No strong pathogenetic dependencies have been identified in GBM, whereas these tumors are characterized by high phenotypic plasticity [3]. Epigenetic deregulation is a key feature of tumor development enhancing phenotypic plasticity and thereby contributing to all hallmarks of cancer [4]. In an effort to identify epigenetic vulnerabilities in GBM, we identified the HIV-1 Tat interactive protein 2 gene (*HTATIP2),* encoding HTATIP2 also called TIP30 or CC3, as aberrantly methylated. *HTATIP2* promoter methylation has also been reported in other tumor types [5, 6, 7, 8, 9], and found most commonly in glioblastoma and low grade glioma, with 70 to over 80% prevalence, according to a pan-cancer analysis [10]. HTATIP2 has a reported inhibitory function on importin b-mediated cytoplasmic-nuclear shuttling of cargo proteins [11], suggesting that epigenetic silencing may affect tumor biology by disturbing the balance of nuclear/cytoplasmic localization of a subset of proteins.

Here we aimed at elucidating the impact of epigenetic silencing of *HTATIP2* on the biology of glioblastoma, mediated by potential aberrant regulation of subcellular localization of cancer relevant

proteins. We selected N-Methylpurine-DNA Glycosylase **(MPG**) as a potentially treatment relevant candidate affected by *HTATIP2* silencing in glioblastoma. MPG recognizes DNA lesions induced by alkylating agents, N7-meGuanin, N3-meGuanin, and N3-meAdenin that constitute the majority of DNA adducts, and initiates the first step of Base Excision Repair (BER) [12, 13]. Furthermore, MPG contains a classic nuclear localization signal (KKQRP), predicting nuclear import via the classic importin α/β1 pathway as suggested by protein localization predictions (WoLF PSORT) [14, 15]. An association of MPG with resistance to alkylating agent therapy in GBM has been reported in a previous study [16].

Here we report on the mechanism by which *HTATIP2* silencing contributes to treatment resistance of GBM cells to treatment with alkylating agents. Downregulation of HTATIP2 in GBM cells shifted the subcellular localization of MPG from cytoplasmic to nuclear localization, thereby enhancing the DNA repair capacity in response to alkylating agents. This modulation was mediated by the capability of HTATIP2 to block cytoplasmic to nuclear translocation of the DNA repair enzyme MPG.

Methods

Data-sets and data processing

The gene expression and DNA methylation data from our glioblastoma patient cohort have been published previously [17, 18] and are available in the Gene Expression Omnibus (GEO) database [http://www.ncbi.nlm.nih.gov/geo/] under the accession-numbers GSE7696 and GSE60274. Expression data was normalized by the RMA procedure (R package limma). The CpG probes with detection p-values > 0.01, located on the sex chromosomes, or in SNPs were removed. The functional normalization was performed by the function preprocessFunnorm from the R package minfi [19]. DNA methylation was summarized by Beta-values [20]. The annotation is based on genome assemblage hg19 (UCSC annotation) and the graphics were produced with R packages Gviz, ggplot2 and cowplot. R (URL http://www.R-project.org) [21].

Cell culture

The GBM cell lines LN-229 (RRID:CVCL_0393), LN-Z308 (RRID:CVCL_0394), and LN-428 (RRID:CVCL_3959) were established in our laboratory according to institutional directives, approved by the Ethics Committee of the Canton de Vaud (CER-VD, protocol F25/99) [22]. BS-153 (RRID:CVCL_S444) was a kind gift from the laboratory of Adrian Merlo [23]. All cell lines were regularly tested to be mycoplasm-free (MycoAlert Kit Lonza, Cat. LT07-418) and were authenticated in 2022 by STR profiling at the Forensic Genetics Unit of the University Center of Legal Medicine, Lausanne and Geneva [24] Cells were cultured in Dulbecco's Modified Eagle Medium (DMEM + GlutaMax, Gibco 61965-026) supplemented with 5% Fetal Calf Serum (FCS, HyClone) at 37°C, 5% CO2. Blasticidine (R21001, Thermofisher) and puromycine (P8833, Sigma) 0.5µg/mL were supplemented to maintain selection of transduced cells

(inducible cells for HTATIP2, anti-*MPG* and anti-*HTATIP2* shRNAs, respectively). To sustain inducibility and avoid leakiness of the inducible systems over time, we used fresh cells from stock every 2-3 months.

Vector Cloning

The recipient vector pCW22 (kindly shared by Prof Joachim Lingner, EPFL [25]) was digested with Sal-I and Sbf-I to remove the Cas9 gene (4kb) from the trAT(Tet-On)-containing plasmid (9.6kb). The donor vector pEGFP-C2 that encodes the canonical isoform 1 of HTATIP2 (CC3, UniProtKB/Swiss-Prot, Q9BUP3-1) [26] was kindly provided by Prof. Hua Xiao, University of Michigan. The plasmid was digested by EcoRI and BamHI to isolate the insert, containing *GFP* (717bp) fused with *HTATIP2* (744bp), and was gel purified (QIAquick® Gel purification kit, Qiagen). The recipient vector and the isolated HTATIP2/GFP sequence were digested with Bam-II and Sal-I to generate compatible ends, and the fragments were ligated using T4 DNA ligase (Promega) (100mg total DNA/ reaction, ratio 1:3). Ligation products were transformed into One Shot® TOP10 Chemically Competent E. *coli* (ThermoScientific, C404010) using the protocol from the manufacturer. Surviving bacterial colonies were tested with PCR for the presence of the *HTATIP2/GFP*-insert, followed by sequence verification (primer sequences, Supplementary Table S1). The pCW22 vector containing the *HTATIP2/GFP*-inducible system was produced in E. *coli* and purified using the QIA plasmid miniprep kit (QIAGEN,12163) for lentiviral production.

Lentiviral production and transduction

For lentiviral production, packaging cells, HEK 293 (kindly provided by Tatiana Petrova's lab) were seeded with 2.5 million cells per 10-cm petri dish for 24h (DMEM, 10% FCS). The Lipofectamin 3000 transfection Kit (Invitrogen, L3000-001) was used. In brief, 2 tubes were prepared, tube A containing 500 µL Optimem medium (31985-062, Lifetechnologies) with 14 µL Lipofectamin 3000, and tube B containing 500 µL Optimem medium, 12 µL P3000 reagent, and three plasmids, with a total of 4.6ng DNA per petri dish. Of note, three plasmids including the expression vector, the packaging vector - pCMV8.74 (Addgene, 22036), and the envelop vector - pMD2.G (Addgene, 12259) were used in a ratio 1:3:4 by DNA weight. The mixture was incubated at RT for 20min, then the content of tube A was transferred to tube B, and incubated for 15min at RT. The medium was aspirated from the HEK 293 cells, and the final mixture was added to the cells. An additional 2ml of Optimem were added to cover the cells. Cells were incubated for 6h before changing with new complete medium. Virus-containing medium was harvested after 24h, passed through a 0.22µm filter (Milan, SCGPT05RE), and complemented with protamin sulfate (10µg/ml). This medium was then added to the target cell plates. Target cells were seeded 24h before transduction, and cells were subjected to antibiotic selection 2 days after transduction.

Doxycycline inducible system for *HTATIP2*

The transduced cells underwent selection with Blasticidine 10µg/mL (R21001, Thermofisher) for 2 weeks. The cell population was then induced with Doxycycline (Dox) (D9891-1G, Sigma Aldrich) for 48h and GFP-positive single cells were sorted by FACS into a 96-well plate containing DMEM with 20% FBS. These plates were then maintained in cell culture for 3-4 weeks. 50µl fresh medium was added weekly. Of note, GFP-tagged HTATIP2 will be turned off after 6 days without Dox. Surviving clones were analyzed by Incucyte Zoom 2016A (Essen Instruments. Version: 3.4) for characterization of cell growth, inducibility and titration of Dox. Dox concentration of 250ng/ml was selected to induce *HTATIP2* unless otherwise indicated, mRNA and protein levels were confirmed by qPCR and Western blot.

IPTG inducible system for anti-*MPG* shRNA and anti-*HTATIP2* shRNA

The Isopropyl β-D-1-thiogalactopyranoside (IPTG) inducible system, uses IPTG (mimics allolactose), to remove a repressor from the lac operon to induce gene expression. Expression vectors pLKO-puro-IPTG-3xLacO, containing nonspecific control shRNA sequence (Sigma, SHC332-1EA) or one of the three specific sequences for anti-*MPG* shRNA (Supplemental Table S2) obtained (SigmaAldrich, Trust in MISSION® Custom Services) and were transfected into TOP10 bacteria to amplify and purify plasmids. Lentiviral production was performed as described above; target cells were LN-229-C25^{HTATIP2Dox} and BS-153-C01^{HTATIP2Dox} (derived by the procedure described in the previous paragraph). Successfully transduced cells were selected by puromycin (P8833, Sigma) 0.5µg/mL. Cells were treated with increasing concentrations of IPTG 0µM, 250 µM, 500µM, 1000µM for 48h, and MPG expression levels were determined by Western blot. The same procedures were followed for the transduction of cells with endogenous HTATIP2 expression (LN-428, LN-Z308) using IPTG-inducible anti-*HTATIP2* shRNAs (Supplemental Table S2).

siRNA transfection

Cells with endogenous HTATIP2 expression (e.g. LN-428, LNZ-308) were transfected with anti-*HTATIP2* siRNA using the Neon electroporation system and kit (Thermofisher, MPK-10025) according to the manufacturers recommendations (1400V, 2ms, 1 pulse). The siRNAs included Silencer™ Select Negative Control No. 1 siRNA (ThermoFisher, 4390843), and the specific anti-HTATIP2 siRNAs: s30128, s30129, and s30700 (ThermoFisher, 4392420).

Live-cell imaging

Live cell imaging was performed using IncuCyte Zoom S3 2016. Cells were seeded into 96-well plates (3596, Corning) at a density of 2500 cells/well (LN-229-C25) and 3000 cells/well (BS-153-C01), respectively. After 24h the cells were treated as indicated in the respective experiments. For cell growth

and cell death, the cells were subjected to pretreatment with Dox or ITPG for 48h to induce the *HTATIP2* or the shRNA of interest, followed by Methylmethansulfonat (MMS) (Sigma, 129925-5G) treatment. For monitoring of cell death, IncuCyte™ Cytotox Red Reagent (Essen BioScience, 4632) was added to the plate at a final concentration of 250nM immediately after MMS treatment. The plate was then transferred into the IncuCyte incubator and the cells were monitored taking images at a 10x magnification every 2 or 3h for 4 days in different channels. Phase contrast was used to determine cell proliferation, Green, for the detection of GFP-tagged HTATIP2, and the Red channel for determination of cell death (Cytotox). Each value is the mean of three technical replicates. The experiments were repeated three times.

Protein extraction and Western Blot

The cells were trypsinized for 2min, neutralized with cold medium, centrifuged, and the cell pellet was snap-frozen in liquid nitrogen, and stored at -80°C until further use. Western blots were performed as previously describe [27]. In brief, protein extracts (20-40µg) were separated on SDS polyacrylamide gradient gels (4-20%, Bio-Rad, 456-1086) and transferred to a nitrocellulose 0.45µm blotting membrane (Bio-Rad, 162-0115). The membranes were incubated with respective primary Abs overnight at 4°C and subsequent with the corresponding secondary HRP-conjugated Abs for 45min at RT. The list of primary and secondary antibodies, and their dilutions are specified in Supplementary Table S3.

Nuclear and cytoplasmic fractionation

Cells were seeded on 10cm petri plates at a density of 0.8 million cells/plate. After 24h the medium was changed and cells were induced with 250ng/mL Dox for 48h. The cells were washed with PBS, followed by adding the lysis buffer of the fractionation Kit, complemented with phosphatase inhibitor and protease inhibitors (Thermo Scientific™ Halt™ Protease Inhibitor Cocktail, Halt™ Phosphatase Inhibitor Cocktail)) directly on the plate, and kept immediately on ice. The NE-PER Nuclear and Cytoplasmic Extraction Kit (ThermoFischer™,78833) was used, according to the manufacturer's instructions, followed by Western blot analysis.

RNA Extraction, qRT-PCR

RNA extraction and qRT-PCR was performed as previously reported [27] using the primer sequences summarized in Supplementary Table S1. Expression was normalized to *GAPDH*.

Confocal microscopy and high content screening imaging

Cells were seeded on different formats, 6-well plates, 8 well-slides, 6-channel -Slide (Ibidi, 80606-IBI), 96-well plates (Operetta, Perkin Elmer) at defined densities. Cells were treated with 250ng/ml Dox, Importin β

inhibitors such as INI-43 (Sigma, SML1911-5MG), or Importazole (Sigma, SML0341-5MG) for 48h. At the defined time points, cells were fixed, permeabilized, and stained with Abs (Supplementary method for details). Image acquisition was performed with a Zeiss LSM 880 Airyscan confocal microscope at 40x magnification (Cellular Imaging Facility, UNIL). Settings included 4 color channels/excitations: DAPI (408nm, Blue), GFP (488nm, Green), MPG/Alexa Fluor 555 (548 nm, Red), P-H2AX/Alexa Fluor 647 or KPNB1/ Alexa Fluor 647 (633nm, Far red). Fifteen images were acquired for each condition for quantification analysis with Cell Profiler.

P-H2AX signal in response to the treatment of increasing MMS concentrations (0- 500nM) and increasing *HTATIP2* induction (Dox+, 0- 500ng/mL) were acquired in a 96-well plate format by high content screening imaging (Operetta, Perkin Elmer) at distinct time points. Nine images were acquired per well, one well per treatment condition. Quantification of the P-H2AX signal was performed by Cell Profiler software.

Image analysis and data processing

The images acquired with confocal microscopy or high content screening (Operetta, Perkin Elmer) were exported as TIF files for Cell Profiler - an open source image analysis software (version 2.2.1, https://github.com/CellProfiler/CellProfiler/releases?page=4). In addition, for Operetta, the background was subtracted from the image using ImageJ before the analysis with Cell Profiler. A pipeline including metadata identity, object recognition, and calculation steps were optimized (see supplementary methods for details). After computation, the parameters of interest were selected and exported into excel format (for P-H2Ax analysis) or as properties files (nuclear translocation analysis). From the excel file, the number of cells, and integrated intensity of P-H2Ax were used for analyses. The properties file was subjected to the Cell Profiler Analyst software in which a machine-learning-based approach is implemented. As result, 2 CSV files were generated. From that, the p enrichment score or ratio of cytoplasmic/nuclear MPG [28, 29] was plotted by Prism for the final graph. Accordingly, a positive (cytoplasmic) enrichment score indicated that a majority of cells with predominantly cytoplasmic MPG localization was present in the tested cell population.

Alkylating agent treatment

Cells were seeded, and Dox or IPTG was added after 24h at a final concentration of 250ng/ml and 500ng/ml, respectively, or as indicated, for 48h. New medium, with or without Dox, IPTG, and MMS, at the concentrations indicated, was added. Incubation times were as indicated, taking into account cell doubling times; e.g. LN-229-C25, cell-doubling time 24h, and BS-153-C01, cell doubling time 39h.

Flow cytometry

Cell death and cell survival was analyzed using the Annexin V Apoptosis Detection Kit APC (Life Technologies, 88-8007-72) following the instructions of the manufacturer. Live cells were prepared and stained with PI and Annexin V. Samples were analyzed by FACS canto-1 at the FACS Core Facility of the University of Lausanne (UNIL). For FACS analysis, cells were gated into quartiles according to Annexin V and PI signals: double negative for Annexin V and PI (living cells); Annexin V positive (Early apoptosis), PI positive (necrosis) and double positive for Annexin V and PI (late apoptosis).

For the study of MPG localization, P-H2AX, and the cell cycle profile, cells were harvested, fixed, permeabilized and stained with antibodies and DAPI (supplementary methods). For the quantification of MPG localization (nuclear/cytoplasmic), the MPG/DAPI similarity score was generated for every single cell by IDEAS software. The frequency distributions of these scores under all five experimental conditions were plotted together (supplementary methods).

Comet assay

Cells were harvested at 0.1M cells in 1mL medium for the comet assay (LubioScience STA-355) following the instructions of the manufacturer. Image acquisition was performed on a Leica LMS880 microscope at 20x magnification, with the orientation of the comet from head to tail (left side to right side). At least 15 images were taken for each condition. Analysis was performed with ImageJ, and the Opencomet analysis tool. After the run, every image was visually inspected in order to control for correct recognition of the comets, otherwise, the specific cell (comet) was marked and automatically removed from the final result. To evaluate DNA SSB damage, the tail moment, defined as the distance from the center of the head to the center of the tail, was used for quantification, considering the relative DNA migration and DNA in the comet tail. The DNA damage is proportional to the tail moment. Of note, we used alkaline electrophoresis, which transforms AP sites into SSB, therefore, it detects SSB, AP sites and other alkali-labile DNA lesions [30].

Results

In a genome wide DNA methylome analysis of a cohort of GBM we identified functional methylation of the *HTATIP2* promoter, reflected in a strong negative correlation between expression and methylation (Figure 1A). The reported regulatory function of HTATIP2 on cytoplasmic-nuclear transport of proteins incited us to investigate the repair enzyme MPG as a treatment relevant candidate, based on our previous observation of predominantly nuclear or cytoplasmic localization of MPG in a subset of GBM [16] (Fig 1B). In order to assess a potential association between epigenetic silencing of *HTATIP2* with MPG subcellular localization, we revisited the readings of MPG immunohistological staining in our cohort of GBM obtained on a tissue micro array [16, 17]. For this analysis, we selected only GBM that were classified with predominantly nuclear or cytoplasmic MPG expression, respectively, excluding samples with both cytoplasmic and nuclear staining. For a limited number of samples, overlapping DNA methylome (HM-450 k) and RNA expression (HG-133Plus2.0 Affymetrix) data were available. Aberrant methylation of the

CpG island, situated in the promoter region of *HTATIP2,* was higher in the GBM classified as expressing nuclear MPG as compared to those with predominantly cytoplasmic MPG expression, as visualized in Figure 1A. In line, there was a significant difference in *HTATIP2* expression between glioblastoma with nuclear MPG versus cytoplasmic MPG expression (p=0.022, Wilcoxon test). GBM exhibiting nuclear MPG expressed less *HTATIP2* than those with cytoplasmic MPG (Figure 1C).

These findings supported our hypothesis that *HTATIP2* may be involved in regulating the subcellular localization of MPG, thereby influencing the DNA repair capacity of GBM cells and their resistance to alkylating agent therapy.

HTATIP2 expression modulates MPG subcellular localization

To address the functional relationship between HTATIP2 expression and MPG subcellular localization, we used GBM cell lines (LN-229, BS-153) lacking endogenous *HTATIP2* expression due to promoter methylation, and transduced them with an inducible, GFP tagged *HTATIP2* construct (TET-ON). Both lines displayed a Doxycycline (Dox) dose-dependent induction of HTATIP2-GFP, while no effect was observed on cell proliferation in the dose range of 0-500ng/ml, monitored by IncuCyte Imaging over a time course of 100h (Supplementary Figure S1). Total MPG was not affected by modulation of HTATIP2 (Figure 2A). Dox-induced *HTATIP2* expression in LN-229-C25-HTATIP2^{Dox} led to a translocation of MPG from predominantly nuclear to cytoplasmic localization, as demonstrated by nuclear/cytoplasmic fractionation, visualized by western blot and confocal microscopy (Figure 2B, C). The subcellular localization of MPG in function of HTATIP2-expression is visualized in an animated 3D projection reconstructed from confocal microscopy (Supplementary 3D animation 1 and 2). Quantification revealed a significant positive cytoplasmic MPG enrichment score, reflecting MPG retention in the cytoplasm ($p<0.0001$, paired t test, Fig. 2C). This was further supported by FACS associated imaging (ImageStream), demonstrating a negative shift of the nuclear (DAPI) similarity of MPG localization in presence Dox-induced HTATIP2 expression (GFP) (Supplementary Figure S2). These results were confirmed in another inducible clone (LN-229-C07-HTATIP2^{Dox}, not shown). Similar results were obtained in the GBM cell line BS-153-HTATIP2^{Dox}-C01 upon Dox-induced expression of *HTATIP2* ($p<0.0001$, unpaired t test; Figure 2D).

For the reverse experiments, we used cell lines expressing endogenous HTATIP2 (LN-Z308 and LN-428) and depleted *HTATIP2* with siRNAs^{HTATIP2}. A shift from predominantly cytoplasmic to nuclear localization was observed in LN-Z308 upon silencing of endogenous *HTATIP2*, as visualized by immunofluorescence (Figure 2E). The results were reproduced in LN-428 (Supplementary Figure S3; three distinct siRNAs were employed and a siRNA-control, efficiency up to 90% reduction of *HTATIP2* RNA).

HTATIP2 acts as inhibitor of nuclear receptors attenuating nuclear localization of MPG

HTATIP2 localizes prominently in proximity to the nuclear membrane area and appears to co-localize with importin β1 (Karyopherin Subunit Beta 1, KPNB1), while excluding MPG from the co-localization area, as visualized by confocal microscopy (Figure 3A). Upon treatment with pharmacologic inhibitors of importin β1, such as Importazole and INI-43, we made the same observation of exclusive localization of Importin

β1 and MPG in absence of HTATIP2 (Figure 3A). The quantification of the subcellular localization of MPG revealed a significant cytoplasmic MPG enrichment score after treatment with the importin β1 inhibitors Importazole and INI-43, hence pheno-copying the effect of HTATIP2 expression (both, $p<0.0001$, unpaired t test; Figure 3B & C). Mechanistically, this is consistent with binding of HTATIP2 to importin β1, as has been suggested based on the crystal structure and pull down experiments [7, 11] that may cause steric hindrance of the cargo protein binding site of importin β1. This precludes binding of importin β1 to MPG via the adapter importin α. Consequently, HTATIP2 may compete with MPG for importin β1 binding, thereby attenuating MPG nuclear transport, in accordance with the exclusion of MPG from HTATIP2-importin β1 co-localization areas. This is in line with previous studies evoking an inhibitory role of HTATIP2 on nuclear translocation of KPNB1 [11], supported by our findings of significant effect on the cytoplasmic/nuclear ratio of KPNB1 upon induction of HTATIP2 expression ($p<0.0001$, t-test, Supplementary Fig S4). Together, these findings support the notion that HTATIP2 may block nuclear translocation of MPG by sequestering importin β1.

HTATIP2 reduces the ratio of nuclear MPG/DNA polymerase β

The efficiency of the BER-pathway relies on the stoichiometry between MPG and the DNA polymerase β (DNA Pol β). While MPG efficiently initiates BER, removing alkylated bases, this leaves behind AP sites and SSB that are resolved by BER downstream enzymes, with DNA Pol β as rate-limiting factor (see scheme for BER in Supplementary Figure S5). Hence, if DNA Pol β is underrepresented compared to MPG, these intermediate lesions accumulate and are even more toxic to the cell than the original lesions. Therefore, we investigated the HTATIP2 effect on the balance between MPG and DNA Pol β, which is determinant for the efficiency of the BER pathway [12]. Nuclear/cytoplasmic fractionation revealed that the MPG/DNA Pol β ratio decreased in the nucleus, while it increased in the cytoplasm of Dox-induced HTATIP2 expressing GBM cells (LN-229-C25-HTATIP2^{Dox} and BS-153-C01-HTATIP2^{Dox}; Supplementary Figure S5). This suggested a potential decrease of the DNA repair capacity of the BER pathway due to relative reduced nuclear levels of MPG. Furthermore, this result also implied that the effect of HTATIP2 on nuclear translocation of MPG is different from DNA Pol β. In other words, the HTATIP2 effect on cargo proteins varies, although the importin α/β-mediated nuclear transport affects a wide range of cargo proteins, including most BER glycosylases like MPG, and some downstream effectors of the BER pathway [31, 32].

HTATIP2 reduces the formation of AP-sites / DNA SSB and DSB upon alkylating agent treatment

Next, we aimed at functionally investigating the effect of HTATIP2 on the DNA damage response (DDR) to alkylating agents mediated by BER. Therefore used MMS as a model alkylating agent, as it yields mostly lesions with N-alkylation (N7-meG, N3-meG, and N3-meA) that are recognized and removed by MPG and subsequently resolved by BER, and not by MGMT [13, 33].

First, we investigated the effect of HTATIP2 on DNA repair activity using the alkaline comet assay that detects SSBs and AP-sites. A significant difference ($p<0.0001$, unpaired t-test) was observed upon MMS

treatment for 48h in absence of HTATIP2 expression, with a longer comet tail moment as compared to HTATIP expressing cells (LN-229-C25-HTATIP2^{Dox+}) (Figure 4A & C). HTATIP2 expression (HTATIP2^{Dox+}) on its own had no effect on the tail moment. To evaluate the involvement of MPG in this process, we depleted MPG using an IPTG-inducible system for anti-*MPG* shRNA and evaluated DNA SSB with the alkaline comet assay. The cells were treated with IPTG to induce shRNA5^{MPG} for 48h, followed by MMS treatment (48h). The MMS treatment of MPG depleted cells revealed a significant difference ($p<0.0001$, unpaired t-test; Figure 4B & D), with shorter comet tail moments, suggesting less AP-sites/ DNA SSB than in presence of MPG. No effect on the comet tail moment was observed upon depletion of MPG in absence of MMS treatment. The induction of the control shRNA^{IPTG+} had no impact on MMS induced AP-sites /DNA SSB (Supplementary Figure S6).

Next, we quantified P-H2AX as a surrogate marker for DNA damage / DSBs by FACS in LN-229-C25-HTATIP2^{Dox} and BS-153-C01-HTATIP2^{Dox} cells. Treatment of HTATIP2^{Dox+} expressing cells with MMS revealed a difference compared to the un-induced cells at 24h as quantified by P-H2AX (unpaired t-test: $p=0.0037$, $p=0.0056$ respectively). A smaller proportion of P-H2AX positive cells were detected among MMS-treated, HTATIP2 expressing cells. No difference was observed in absence of MMS treatment in either cell line (Figure 5A, B). Again, similar results were obtained upon depletion of *MPG* in LN-229-C25 and BS-153-C01 with *anti-MPG* shRNA, followed by MMS treatment. The reduction of MPG resulted in less P-H2AX positive cells in both cell lines (Supplemental Figure S7).

In order to evaluate the dose dependence between the expression levels of HTATIP2 and the concentrations of the MMS treatment to induce P-H2AX expression, HTATIP2 was induced in LN-229-C25-HTATIP2^{Dox} cells with increasing amounts of Dox [0-500ng/ml] for 48h, followed by treatment for 24h with increasing concentrations of MMS [0-500nM]. Increasing amounts of HTATIP2 resulted in decreasing levels of P-H2AX in response to the tested dose range of MMS (Figure 5C). Similarly, reduction of MPG in LN-229-C25-shMPG^{IPTG}, using increasing concentrations of IPTG [0-500ng/ml] followed by MMS treatment, showed less DSB than the corresponding control (Figure 5D). In accordance, depletion of endogenous *HTATIP2* in LN-Z308-shHTATIP2^{ITPG} using an inducible shRNA against *HTATIP2* resulted in an increase of DNA damage upon MMS treatment, as measured by P-H2AX (Supplementary Figure S8A).

Taken together, these results suggest that HTATIP2 expression retains MPG in the cytoplasm, and thereby decreases nuclear MPG, reducing the DNA repair capacity, reflected in decreased AP-sites/SSB or DSB. This effect was pheno-copied by depleting MPG. In line, the opposite result was observed when knocking down *HTATIP2* in cells with endogenous expression.

MMS effect on proliferation and cell death modulated by HTATIP2 and MPG

We next studied the effects of HTATIP2 expression on cell proliferation and survival in response to the alkylating agent MMS. We monitored proliferation of LN-229-C25-HTATIP2^{Dox} cells by live cell imaging (IncuCyte) and observed decreased cell proliferation upon MMS (200nM) treatment over the time course of 72h, with a more pronounced reduction of the growth rate in HTATIP2^{DOX+} expressing cells as

compared to their respective controls (Figure 6A). Follow-up experiments revealed differences in cell death at 72h (unpaired t test, p=0.0033, Figure 6B), but not at 24h of MMS treatment. A higher cell death rate was observed in HTATIP2^{DOX+} expressing cells as compared to HTATIP2 non-expressing cells, as quantified by FACS Annexin V-PI analysis. This is in accordance with the separation of the growth curves after only 24h. In absence of HTATIP2, the depletion of MPG by anti MPG shRNA^{IPTG+} pheno-copied the effect of HTATIP2^{DOX+} on cell growth in MMS-treated cells (Figure 6C). This suggested that the effect of HTATIP2 on cell survival upon MMS treatment is mediated by reduction of nuclear MPG. Taken together, HTATIP2^{Dox+} sensitized LN-229 to MMS treatment.

HTATIP2 attenuates MMS-induced cell death at 24h in BS-153 cells

The same treatment scheme was applied to BS-153-HTATIP2^{Dox}. In contrast to LN-229, we observed an earlier response to MMS treatment, reflected in cell death that peaked at 24h as monitored by live-cell imaging, regardless of HTATIP2 expression. The amplitude of cell death was attenuated in HTATIP2 expressing cells (Dox+) (Figure 6D), in accordance with the growth curve (Supplementary Figure S9). This difference was confirmed by FACS Annexin V-PI analysis, showing a higher percentage of dead cells after 24h of MMS treatment in cells not expressing HTATIP2 (Figure 6E). This pattern of response to MMS treatment was pheno-copied by depletion of MPG (shRNA^{IPTG+}) in the absence of HTATIP2 expression (Figure 6F). This suggests that BS-153 cells were partially protected from toxicity of MMS-treatment in presence of HTATIP2 (Figure 6DE) or absence/depletion of MPG, respectively (Figure 6F).

Subsequent cell cycle analyses revealed an expected MMS-induced disturbance of the cell cycle. We observed a trend (p=0.051) for a HTATIP2 dependent modulation of the MMS induced cell cycle change in LN-229, with a similar change in the profile upon depletion of MPG. This is consistent, with the observed attenuation of MMS associated p21 induction in presence of HTATIP2. For BS-153 the cycle profiles were not modulated by HTATIP2 expression, or depletion of MPG (supplementary Figure S10). Of note, LN-229 has wild-type p53 function, in contrast to the other two cell lines.

Discussion

In this study, we aimed at elucidating the biological role of HTATIP2 in GBM that displayed frequent epigenetic silencing through gene promoter methylation. A regulatory function in cytoplasmic to nuclear translocation of proteins has been attributed to HTATIP2, mediated by physical interaction with importin βs [11]. Therefore, we hypothesized that epigenetic silencing of *HTATIP2* may modulate nuclear transport of cancer relevant proteins in an importin β-dependent manner.

We focused our attention on the DNA repair protein MPG as a potential cancer relevant target of HTATIP2. Inspection of the MPG sequence revealed a classical NLS, predicting nuclear transport via the importin alpha/beta 1 pathway. In contrast, MGMT is not predicted to comprise such a NLS (WoLF PSORT) [14]. Furthermore, we had previously reported an association between nuclear MPG expression and shorter

survival in GBM patients, suggesting a contribution of MPG to treatment resistance to alkylating agent therapy [16, 34].

First, we substantiated the hypothesized association between subcellular localization of MPG, and expression of *HTATIP2* in a panel of GBM, which incited us to investigate underlying mechanisms. Modulation of HTATIP2 expression in GBM cell lines confirmed a functional relationship. GBM cell lines lacking HTATIP2 expression displayed nuclear MPG that was shifted to predominantly cytoplasmic localization upon induction of HTATIP2 expression. In accordance, the inverse relationship was observed when performing the opposite experiment: depletion of HTATIP2 in GBM cells with endogenous HTATIP2 expression shifted MPG from cytoplasmic to nuclear localization. No evidence for a direct effect on cell proliferation was observed when inducing *HTATIP2* expression in a dose dependent manner in these GBM cell lines under standard conditions.

HTATIP2 co-localized with importin β1 in proximity to the nuclear membrane, in line with their reported physical interaction [11], while MPG was excluded from this area and remained in the cytoplasm. In support of this relationship, we demonstrated that pharmacologic inhibitors of importin β1 also retained MPG in the cytoplasm in absence of HTATIP2. This suggests that HTATIP2 functions as a negative regulator of nuclear MPG function by sequestering importin β1. This is also supported by the steric hindrance of HTATIP2 on the cargo binding site that has been shown for importin β2, based on the crystal structure [7].

The cellular response to silencing of HTATIP2 will depend on the cell type-specific proteome, given its known regulatory function on cellular protein shuttling. Importantly, the effect will become evident under stress conditions in which HTATIP-regulated proteins become rate limiting for the stress response. Here we applied genotoxic stress to the cells by treatment with an alkylating agent that revealed the crucial function of MPG as initiator of BER. We used MMS as a model alkylating agent as it yields mostly lesions with N-alkylation (95% of the total alkylations, N7-meG, N3-meG, and N3-meA) that are repaired by BER and not by MGMT [13, 33]. These lesions, recognized and removed by MPG, leave behind toxic intermediates (AP-sites) if not immediately converted in subsequent steps of BER [35]. Hence, the HTATIP2-induced cytoplasmic retention of MPG decreased the MMS induced formation of AP-sites and resulting DNA SSB/ DSB, concordant with reduced P-H2AX formation in all models tested, suggesting attenuated DNA repair capacity. This phenotype of reduced formation of P-H2AX was mimicked by depletion of MPG in absence of HTATIP2, providing evidence for the MPG specificity of the observed effect, and supporting the central role of MPG in this process. Consequently, silencing of *HTATIP2* enhances the inherent DNA damage response to alkylating agent therapy. The cytoplasmic retention of MPG, compromising DNA repair capacity, may therefore attenuate DDR signaling, reducing immediate cell death, and leave behind unrepaired DNA lesions. Subsequent DNA translesion synthesis - ignoring DNA lesions – may result in mutations as trade-off. Alternatively, unsolved DNA lesions may block the replication fork, and may induce Sister Chromatide Exchange (SCE) mediated repair, resulting in genome instability. However, the consequences on downstream events relevant for cell fate certainly depends, in addition, on the patho-

genetic make-up of the cells including, but not limited to, p53 function, as reported by others. The HTATIP2-mediated attenuation of p21 induction by MMS in the p53 proficient cell line LN-229, may be due to the associated reduction of DDR signaling, attenuating the MMS-induced cell cycle arrest, leaving lesions unrepaired, and subsequently leading to an apparent sensitization of the cells to MMS in presence of HTATIP2. The importance of p53 function for the resistance to alkylating agents has been reported in detail by others, including for LN-229 [36, 37].

Taken together, this study sheds light on a new mechanism of treatment resistance to alkylating agents affecting GBM patients. The epigenetic silencing of *HTATIP2* in GBM abrogates the physiologic negative regulatory effect on nuclear translocation of MPG, enhancing the DNA repair capacity and thereby diminishing the treatment effect. This is a timely finding in the context of recent efforts of directly targeting nuclear import/export of proteins in preclinical studies and clinical trials for GBM patients [38, 39, 40].

Declarations

Acknowledgements

We acknowledge and thank Pierre Bady for providing Figure 1, and thank the collaborators of the FACS and the Core Imaging Facility (CIF) of the University of Lausanne, and the high content imaging at BIOP, at the Federal Institute of Technology Lausanne (EPFL) for excellent technical support. The Graphical abstract and the Supplemental Figure S5C were created with BioRender.com.

Conflict of interest statement:

No conflicts of interest to report.

Authorship Contribution Statement:

TN and MEH designed the study. TN performed the experiments, analyzed and interpreted the data, and wrote the manuscript with MEH. PR and KVD contributed preliminary experimental data. MDTP, LW, AJ, and MCB performed experiments and analyzed data. MEH directed the study. All authors contributed to manuscript writing.

Ethics Statement:

The glioblastoma derived cell lines were established in our lab according to institutional directives, approved by the Ethics Committee of the Canton de Vaud, Lausanne, Switzerland (CER-VD, protocol F25/99; Brain tumor biobank, BB_031BBLGBT).

Funding Statement:

This work was supported by the Swiss National Science Foundation (SNSF 31003A_182821) and the Krebsforschung Schweiz (KFS-4461-02-2018).

References

1. Stupp R, Hegi ME, Mason WP, van den Bent MJ, Taphoorn MJ, Janzer RC*, et al.* Effects of radiotherapy with concomitant and adjuvant temozolomide versus radiotherapy alone on survival in glioblastoma in a randomised phase III study: 5-year analysis of the EORTC-NCIC trial. *Lancet Oncol* 2009, **10**(5)**:** 459-466.
2. Weller M, van den Bent M, Preusser M, Le Rhun E, Tonn JC, Minniti G*, et al.* EANO guidelines on the diagnosis and treatment of diffuse gliomas of adulthood. *Nat Rev Clin Oncol* 2021, **18**(3)**:** 170-186.
3. Chaligne R, Gaiti F, Silverbush D, Schiffman JS, Weisman HR, Kluegel L*, et al.* Epigenetic encoding, heritability and plasticity of glioma transcriptional cell states. *Nat Genet* 2021, **53**(10)**:** 1469-1479.
4. Hanahan D. Hallmarks of cancer: New dimensions. *Cancer Discov* 2022, **12**(1)**:** 31-46.
5. Zhao J, Chen JJ, Lu B, Dong L, Wang HJ, Bi CS*, et al.* TIP30 induces apoptosis under oxidative stress through stabilization of p53 messenger RNA in human hepatocellular carcinoma. *Cancer Research* 2008, **68**(11)**:** 4133-4141.
6. Zhu M, Yin F, Fan X, Jing W, Chen R, Liu L*, et al.* Decreased TIP30 promotes Snail-mediated epithelial-mesenchymal transition and tumor-initiating properties in hepatocellular carcinoma. *Oncogene* 2015, **34**(11)**:** 1420-1431.
7. El Omari K, Bird LE, Nichols CE, Ren J, Stammers DK. Crystal structure of CC3 (TIP30): implications for its role as a tumor suppressor. *J Biol Chem* 2005, **280**(18)**:** 18229-18236.
8. Li X, Zhang Y, Cao S, Chen X, Lu Y, Jin H*, et al.* Reduction of TIP30 correlates with poor prognosis of gastric cancer patients and its restoration drastically inhibits tumor growth and metastasis. *Int J Cancer* 2009, **124**(3)**:** 713-721.
9. Dong X, Deng Q, Nie X, Zhang M, Jia W, Chen C*, et al.* Downregulation of HTATIP2 expression is associated with promoter methylation and poor prognosis in glioma. *Exp Mol Pathol* 2015, **98**(2)**:** 192-199.
10. Saghafinia S, Mina M, Riggi N, Hanahan D, Ciriello G. Pan-Cancer landscape of aberrant DNA methylation across human tumors. *Cell Rep* 2018, **25**(4)**:** 1066-1080 e1068.
11. King FW, Shtivelman E. Inhibition of nuclear import by the proapoptotic protein CC3. *Mol Cell Biol* 2004, **24**(16)**:** 7091-7101.
12. Krokan HE, Bjoras M. Base excision repair. *Cold Spring Harbor perspectives in biology* 2013, **5**(4)**:** a012583.
13. Kaina B, Christmann M. DNA repair in personalized brain cancer therapy with temozolomide and nitrosoureas. *DNA Repair (Amst)* 2019, **78:** 128-141.
14. Horton P, Park KJ, Obayashi T, Fujita N, Harada H, Adams-Collier CJ*, et al.* WoLF PSORT: protein localization predictor. *Nucleic Acids Res* 2007, **35**(Web Server issue)**:** W585-587.

15. Lange A, Mills RE, Lange CJ, Stewart M, Devine SE, Corbett AH. Classical nuclear localization signals: definition, function, and interaction with importin alpha. *J Biol Chem* 2007, **282**(8)**:** 5101-5105.
16. Agnihotri S, Gajadhar AS, Ternamian C, Gorlia T, Diefes KL, Mischel PS*, et al.* Alkylpurine-DNA-N-glycosylase confers resistance to temozolomide in xenograft models of glioblastoma multiforme and is associated with poor survival in patients. *J Clin Invest* 2012, **122**(1)**:** 253-266.
17. Murat A, Migliavacca E, Gorlia T, Lambiv WL, Shay T, Hamou MF*, et al.* Stem cell-related "self-renewal" signature and high epidermal growth factor receptor expression associated with resistance to concomitant chemoradiotherapy in glioblastoma. *J Clin Oncol* 2008, **26**(18)**:** 3015-3024.
18. Kurscheid S, Bady P, Sciuscio D, Samarzija I, Shay T, Vassallo I*, et al.* Chromosome 7 gain and DNA hypermethylation at the HOXA10 locus are associated with expression of a stem cell related HOX-signature in glioblastoma. *Genome Biol* 2015, **16**(1)**:** 16.
19. Fortin JP, Labbe A, Lemire M, Zanke BW, Hudson TJ, Fertig EJ*, et al.* Functional normalization of 450k methylation array data improves replication in large cancer studies. *Genome Biol* 2014, **15**(12)**:** 503.
20. Du P, Zhang X, Huang CC, Jafari N, Kibbe WA, Hou L*, et al.* Comparison of Beta-value and M-value methods for quantifying methylation levels by microarray analysis. *BMC Bioinformatics* 2010, **11:** 587.
21. R Core Team. A language and environment for statistical computing. 2015 [cited]Available from: http://www.R-project.org
22. Ishii N, Maier D, Merlo A, Tada M, Sawamura Y, Diserens AC*, et al.* Frequent co-alterations of TP53, p16/CDKN2A, p14ARF, PTEN tumor suppressor genes in human glioma cell lines. *Brain Pathol* 1999, **9**(3)**:** 469-479.
23. Jones G, Machado J, Jr., Merlo A. Loss of focal adhesion kinase (FAK) inhibits epidermal growth factor receptor-dependent migration and induces aggregation of nh(2)-terminal FAK in the nuclei of apoptotic glioblastoma cells. *Cancer Res* 2001, **61**(13)**:** 4978-4981.
24. Bady P, Diserens AC, Castella V, Kalt S, Heinimann K, Hamou MF*, et al.* DNA fingerprinting of glioma cell lines and considerations on similarity measurements. *Neuro Oncol* 2012, **14**(6)**:** 701-711.
25. Glousker G, Briod AS, Quadroni M, Lingner J. Human shelterin protein POT1 prevents severe telomere instability induced by homology-directed DNA repair. *EMBO J* 2020, **39**(23)**:** e104500.
26. Ito M, Jiang C, Krumm K, Zhang X, Pecha J, Zhao J*, et al.* TIP30 deficiency increases susceptibility to tumorigenesis. *Cancer Res* 2003, **63**(24)**:** 8763-8767.
27. Vassallo I, Zinn P, Lai M, Rajakannu P, Hamou MF, Hegi ME. WIF1 re-expression in glioblastoma inhibits migration through attenuation of non-canonical WNT signaling by downregulating the lncRNA MALAT1. *Oncogene* 2016, **35**(1)**:** 12-21.
28. Carpenter AE, Jones TR, Lamprecht MR, Clarke C, Kang IH, Friman O*, et al.* CellProfiler: image analysis software for identifying and quantifying cell phenotypes. *Genome Biol* 2006, **7**(10)**:** R100.
29. Stockwell SR, Mittnacht S. Workflow for high-content, individual cell quantification of fluorescent markers from universal microscope data, supported by open source software. *J Vis Exp* 2014(94).

30. Luke AM, Chastain PD, Pachkowski BF, Afonin V, Takeda S, Kaufman DG*, et al.* Accumulation of true single strand breaks and AP sites in base excision repair deficient cells. *Mutat Res* 2010, **694**(1-2)**:** 65-71.
31. Knudsen NO, Andersen SD, Lutzen A, Nielsen FC, Rasmussen LJ. Nuclear translocation contributes to regulation of DNA excision repair activities. *DNA Repair (Amst)* 2009, **8**(6)**:** 682-689.
32. Kirby TW, Gassman NR, Smith CE, Zhao ML, Horton JK, Wilson SH*, et al.* DNA polymerase beta contains a functional nuclear localization signal at its N-terminus. *Nucleic Acids Res* 2017, **45**(4)**:** 1958-1970.
33. Glaab WE, Tindall KR, Skopek TR. Specificity of mutations induced by methyl methanesulfonate in mismatch repair-deficient human cancer cell lines. *Mutat Res* 1999, **427**(2)**:** 67-78.
34. Agnihotri S, Burrell K, Buczkowicz P, Remke M, Golbourn B, Chornenkyy Y*, et al.* ATM regulates 3-methylpurine-DNA glycosylase and promotes therapeutic resistance to alkylating agents. *Cancer Discov* 2014, **4**(10)**:** 1198-1213.
35. Tang JB, Svilar D, Trivedi RN, Wang XH, Goellner EM, Moore B*, et al.* N-methylpurine DNA glycosylase and DNA polymerase beta modulate BER inhibitor potentiation of glioma cells to temozolomide. *Neuro Oncol* 2011, **13**(5)**:** 471-486.
36. Hermisson M, Klumpp A, Wick W, Wischhusen J, Nagel G, Roos W*, et al.* O6-methylguanine DNA methyltransferase and p53 status predict temozolomide sensitivity in human malignant glioma cells. *J Neurochem* 2006, **96**(3)**:** 766-776.
37. He Y, Kaina B. Are there thresholds in glioblastoma cell death responses triggered by temozolomide? *Int J Mol Sci* 2019, **20**(7).
38. Zhu ZC, Liu JW, Li K, Zheng J, Xiong ZQ. KPNB1 inhibition disrupts proteostasis and triggers unfolded protein response-mediated apoptosis in glioblastoma cells. *Oncogene* 2018, **37**(22)**:** 2936-2952.
39. Lassman AB, Wen PY, van den Bent MJ, Plotkin SR, Walenkamp AME, Green AL*, et al.* A phase II study of the efficacy and safety of oral Selinexor in recurrent glioblastoma. *Clin Cancer Res* 2022, **28**(3)**:** 452-460.
40. El-Tanani M, Dakir el H, Raynor B, Morgan R. Mechanisms of nuclear export in cancer and resistance to chemotherapy. *Cancers (Basel)* 2016, **8**(3).

Figures

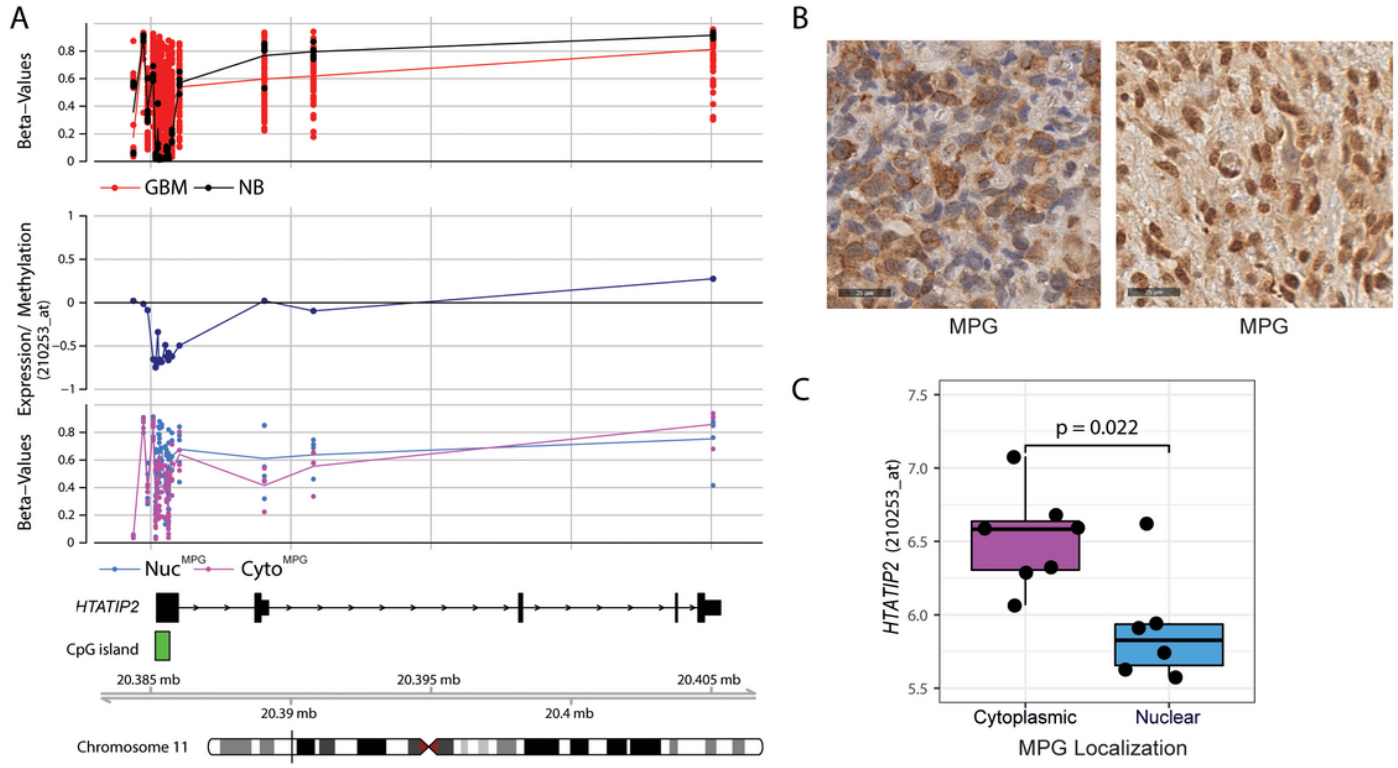

Figure 1

Figure 1

Association of *HTATIP2* methylation and expression with cytoplasmic localization of MPG.

A The β-values of CpG methylation in the promoter of *HTATIP2* is visualized for GBM (n=63, red) and non-tumoral brain (NTB, n=5, black). Highly variable methylation is observed in the CpG island (indicated in green) associated with the *HTATIP2* promoter in GBM, while no methylation is detected in NTB. The functional methylation of the *HTATIP2* promoter is indicated by a negative correlation (Spearman) between *HTATIP2* expression (Affymetrix probe 210253_at, recognizes all transcripts) and DNA methylation (E/M) (black). The association of nuclear (Nuc, blue) versus cytoplasmic (Cyto, pink) MPG localization, classified according to immunohistochemistry [16], and CpG methylation of *HTATIP2* (β-values) is illustrated. **B** Representative GBM displaying predominantly cytoplasmic or nuclear MPG expression, respectively (immunohistochemistry, size bar, 25µm, tissue micro array). **C** Box plot of *HTATIP2* expression (probe 210253_at) in GBM samples, scored as expressing either cytoplasmic (pink) or nuclear MPG (blue) (p=0.022, Wilcoxon test). GBM with both, nuclear and cytoplasmic expression were not included. Overlapping information between GBM samples represented on the tissue micro array, for which DNA methylation, and/or RNA expression was available was limited.

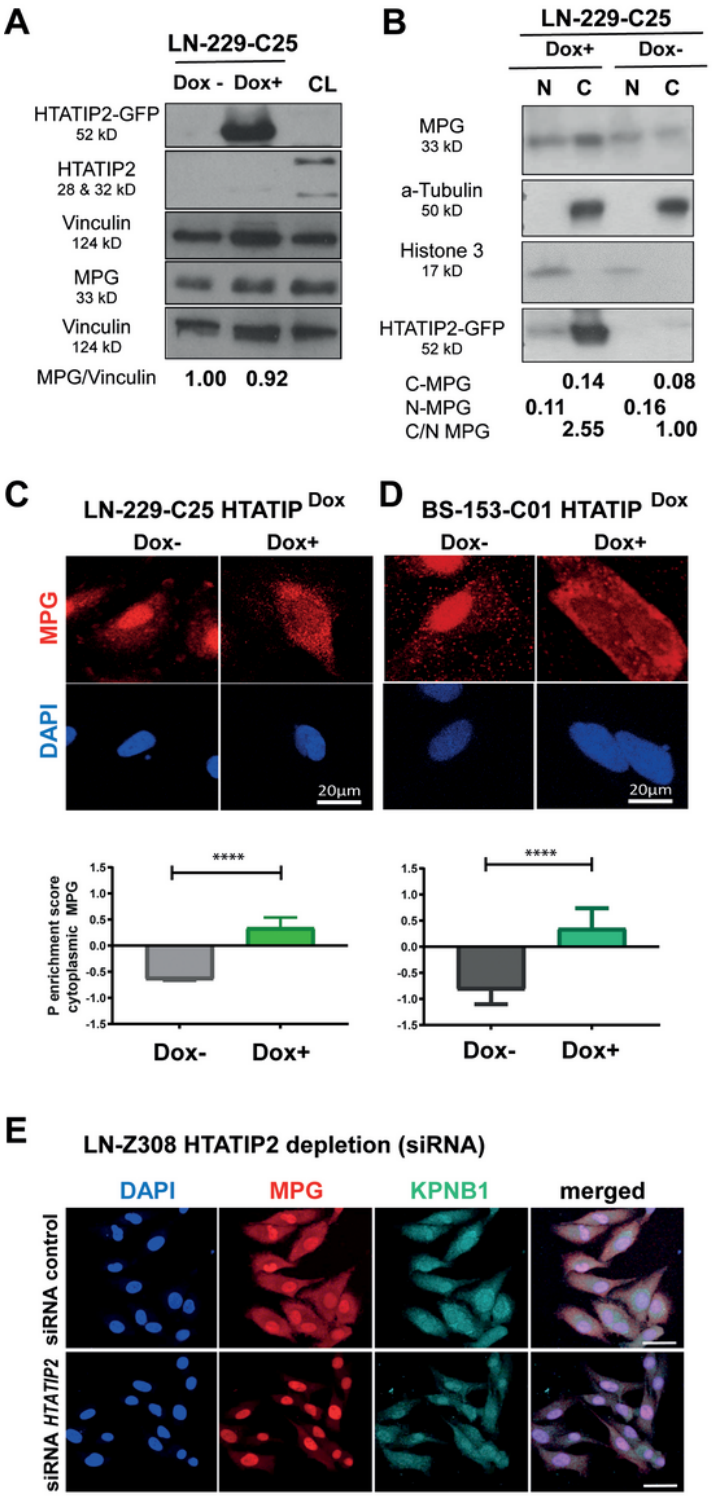

Figure 2

Figure 2

Modulation of HTATIP2 expression affects MPG subcellular localization.

A Expression of the HTATIP2-GFP-fusion protein (52kDa) was induced by Doxycycline (Dox+, 250ng/ml) in clone 25 of LN-229 (LN-229-C25-HTATIP2^{Dox}) for 48h. LN-229 does not express endogenous HTATIP2. Westerns were probed with Ab against HTATIP2, and MPG (33kDa), and were normalized to Vinculin (124

kDa) of the corresponding blots. A cell line (CL) with endogenous HTATIP2 expression served as positive HTATIP2-control (28 and 32 kDa). MPG expression in presence or absence of HTATIP2-induction was quantified by densitometry. **B** LN-229-C25-HTATIP2^{Dox} cells, induced with (Dox+) or not (Dox-), were fractionated and analyzed for relative nuclear (N) and cytoplasmic (C) MPG expression, normalizing the nuclear fraction (N) with Histone 3 (15 kDa) and the cytoplasmic fraction (C) with α-Tubulin (50 kDa). The HTATIP-GFP fusion protein is detected with the anti-GFP anti-body. **C-D** MPG expression visualized by confocal microscopy (scale bar 20µm) in cell lines LN-229-C25-HTATIP2^{Dox} and BS-153-C1-HTATIP2^{Dox} with or without Dox-induced expression of HTATIP2 (48h). The corresponding P enrichment scores for cytoplasmic MPG localization were quantified by Cell Profiler. Experiments were performed in 3 biological replicates (**C**, n=191 cells, total n= 799 cells; **D**, (n=762; total, n= 1734). **E** The localization of MPG expression is shown for LN-Z308 upon silencing of endogenous *HTATIP2* by siRNA (s700) after 48h (scale bar 50µm). Representative images are shown for DAPI, blue; MPG, red; KPNB1, cyan; or merged. LSM 880 microscopy. Cells were visualized by confocal microscopy image using four channels: KPNB1-Alexa 647 (far red), MPG-Alexa 555 (red), and DAPI (blue). Full length Westerns are available in Supplemental Material for **A** and **B**.

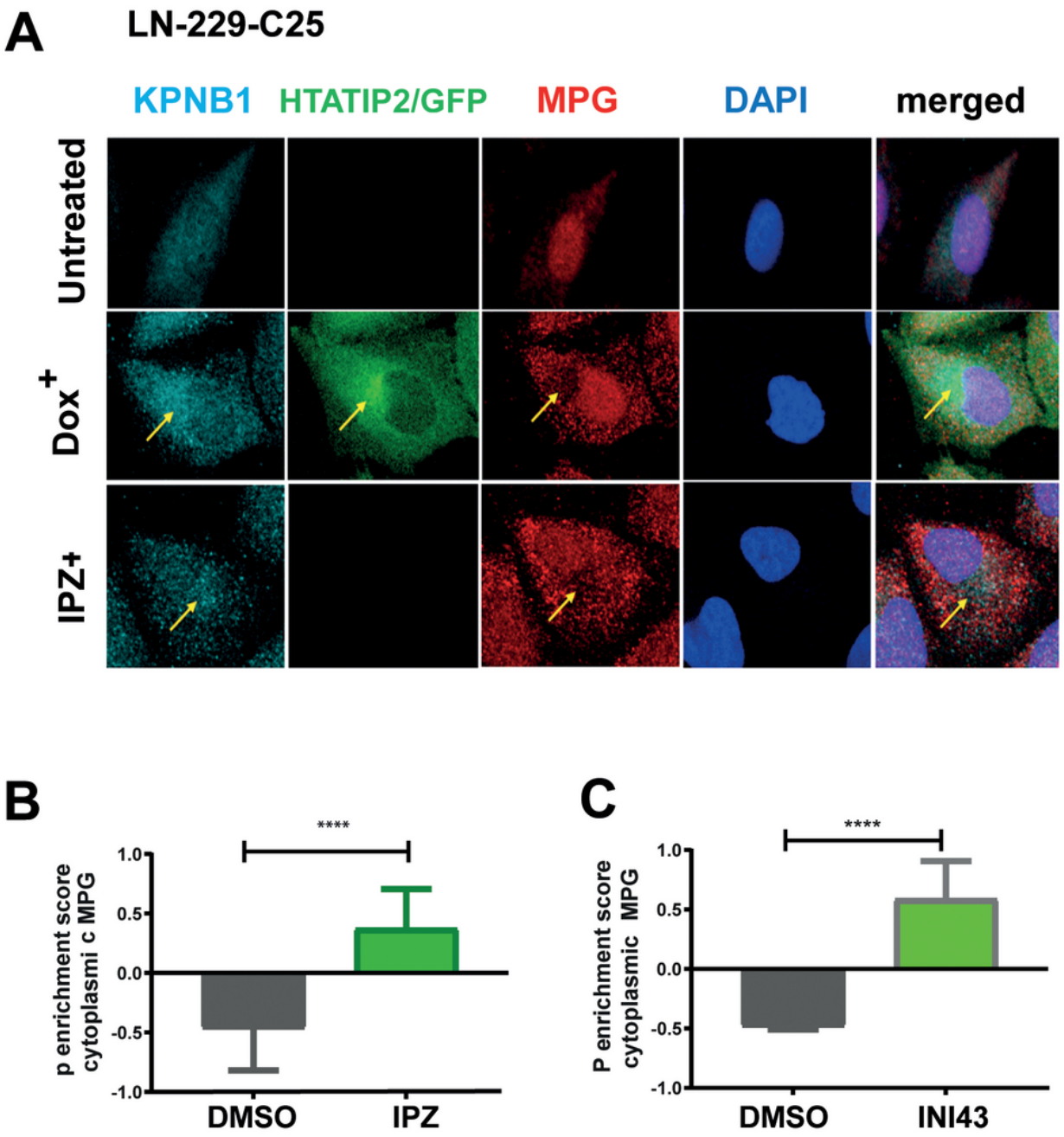

Figure 3

Figure 3

HTATIP2 depletion favors nuclear localization of MPG.

A LN-229-C25-HTATIP2^{Dox} cells were either induced with Dox to express HTATIP2, or treated with 8nM Importazole (IPZ) for 48h. Cells were visualized by confocal microscopy image using four channels: KPNB1-Alexa 647 (far red), GFP (488, green), MPG-Alexa 555 (red), and DAPI (blue). HTATIP2-GFP

localizes mainly in the cytoplasm, with a focus in proximity to the nuclear membrane. HTATIP2 co-localized with importin β1 (KBNB1) at the location where MPG is excluded. Areas of interest are indicated by arrows. **B-C** Quantification of the P cytoplasmic enrichment score for MPG upon treatment with the pharmacologic inhibitors of KPNB1: **G,** IPZ (8nM); **H,** INI-43 (8nM). INI-43 treatment: n= 486 cells, t-test:****(p<0.0001). IPZ treatment: n= 263 cells, t-test:****(p<0.0001). Representative read-out of 3 biological replicates.

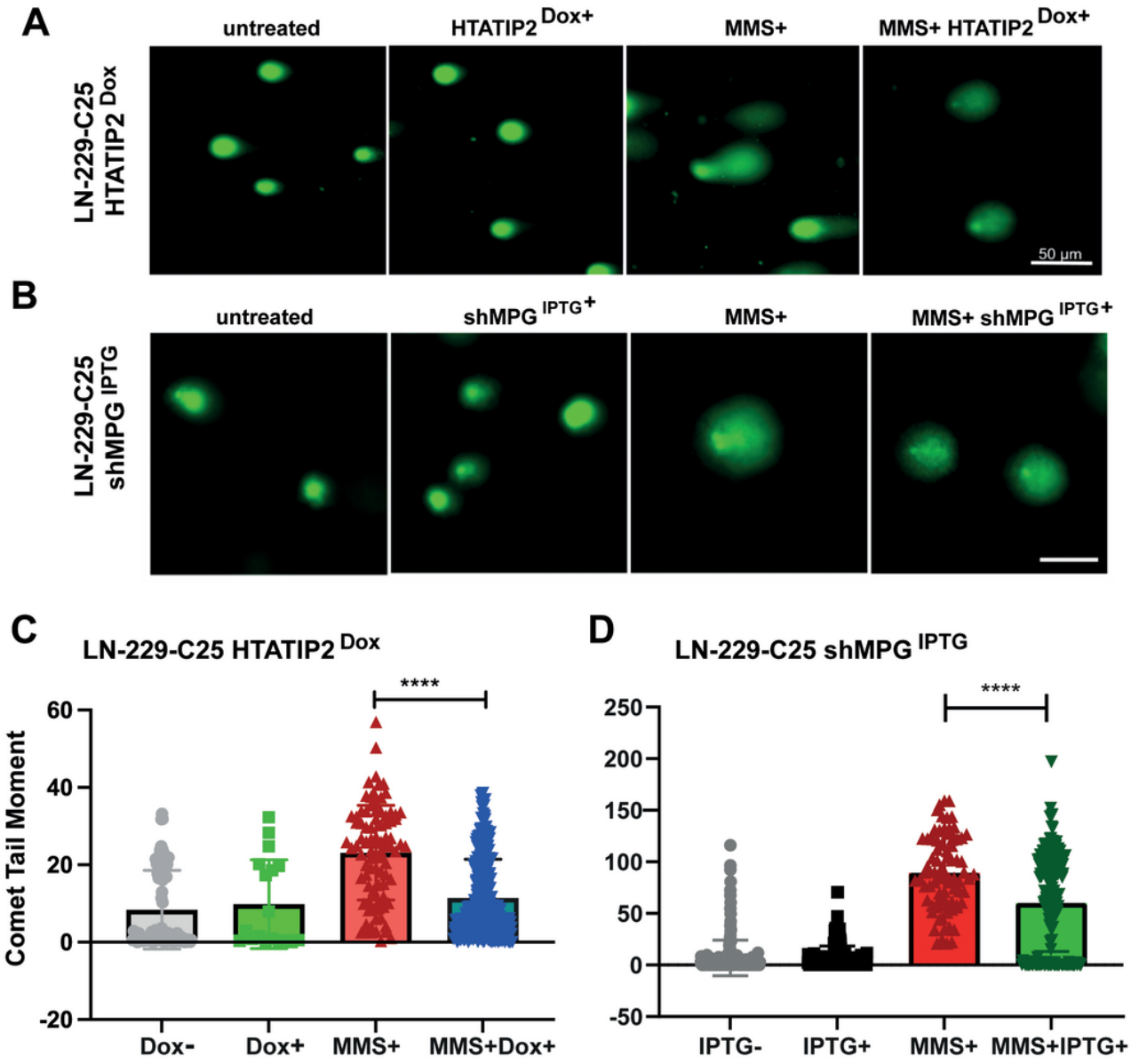

Figure 4

Figure 4

Induction of HTATIP2 or depletion of MPG reduce MMS-induced SSB and AP-sites.

The formation of SSBs and AP sites was evaluated upon induction of HTATIP2 or depletion of MPG using the alkaline comet assay after 48h of MMS treatment. **A** Visualization of the comet tail moment under the four indicated experimental conditions using the Dox-inducible cell line LN-229-C25 for HTATIP2 expression (image scale 50µm), and **B** the LN-229-C25 cell line with IPTG-inducible anti-MPG shRNA5^{IPTG}, image scale 50µm. SSBs and AP sites were quantified as comet tail moment, defined by the distance from the center of the comet head to the center of the comet tail. **C,** Analysis was performed on 478 cells (ImageJ, Fiji, adding Opencomet analysis tool). Treatment conditions: Untreated, grey; Dox [250ng/ml], green; MMS [200nM], red; and combination, blue. **D**. Analysis was performed on a total of 208 images, comprising 713 cells. Treatment conditions: Untreated, grey; IPTG [500ng/ml], black; MMS 200nM, red; and the combination, green. The experiments were performed in triplicate. (**** $p<0.0001$, t-test). Control experiment for anti-*MPG* shRNA with not-targeting shRNA, Supplementary Figure S6.

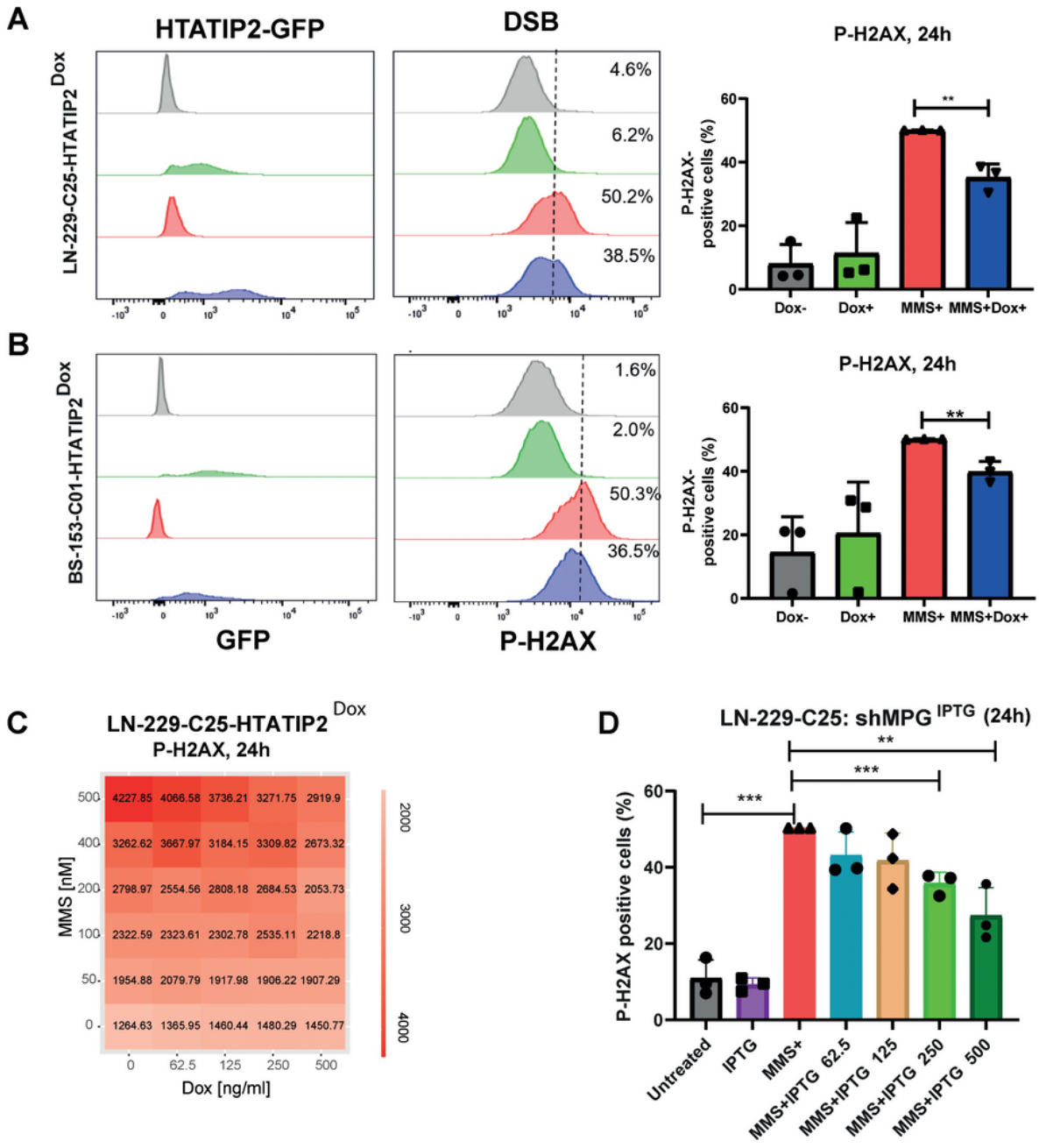

Figure 5

Figure 5

Induction of DSB by MMS in function of HTATIP2 and MPG expression

A Expression of HTATIP2-GFP was induced by Dox in LN-229-25-HTATIP2^{Dox} [250ng/l] and **B** BS-153-01-HTATIP2^{Dox} [500ng/l] cells for 48h, followed by MMS treatment for 24h [200nM and 100nM, respectively]. Cells were subjected to FACS to quantify the P-H2Ax signal and monitor HTATIP-GFP expression. The

threshold was set at 50% for MMS treated cells. The experiments were performed in biological triplicates. (** p<0.01, t-test). **C** A heatmap of P-H2Ax signal in LN-229-25-HTATIP2^{Dox} visualizes the response to the combination treatment of increasing concentrations of MMS [0-500nM] and dose dependent induction of *HTATIP2* [Dox 0-500ng/ml], quantified 24h after treatment with MMS (Operetta high content screening). Decreasing levels of DSB were observed with increasing expression of HTATIP2. **D** MPG was depleted in LN-229-C25-shMPG^{IPTG}, in absence of HTATIP2, using the inducible shRNA5 against *MPG*. LN-229-C25-sh*MPG*^{IPTG} cells were pretreated 48h with ITPG, using a dose range from 0 to 500 ng/ml, followed by treatment with 200nM MMS for 24h. Downregulation of *MPG* significantly altered the formation of DSB, with decreasing P-H2Ax levels detected by FACS. Depletion of *HTATIP2* significantly affected the formation of MMS-induced DSB, reflected in increased levels of P-H2Ax as quantified by FACS. (**D,** analysis of 3 technical replicates, (p<0.5*, p<0.01**, p<0.001***, unpaired t-test).

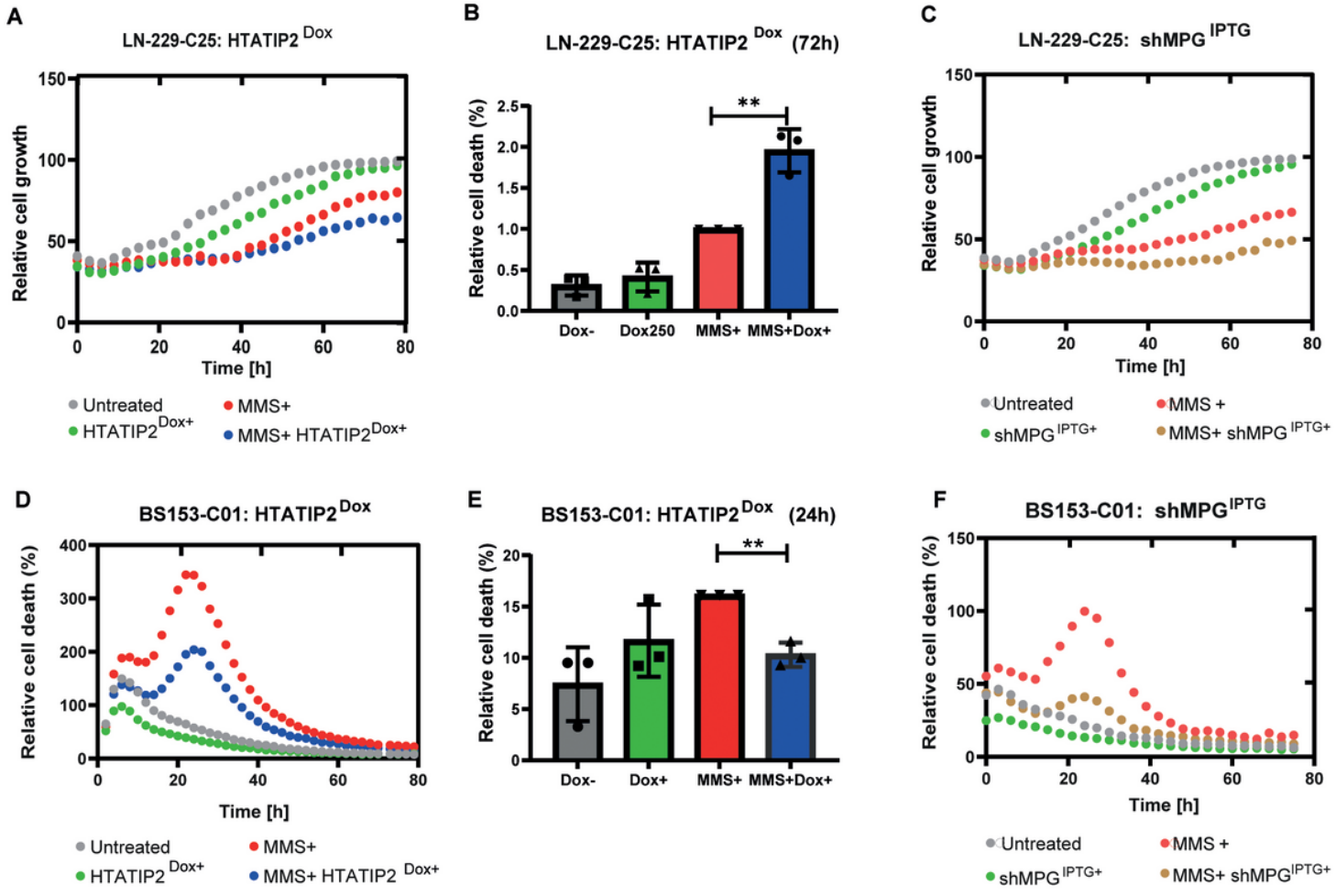

Figure 6

Figure 6

HTATIP2 modulates cell response to MMS treatment

A LN-229-C25-HTATIP2^{Dox} cells were treated with Dox for 48h to induce HTATIP2 expression followed by treatment with MMS. Relative cell growth was determined by monitoring cell confluency over 72h by phase-contrast, taking images every 3h (IncuCyte). Treatment conditions, untreated (grey), Dox [250ng/ml] (green), MMS [200nM] (red), and the combination (blue). **B** Cell death at 72h in response to MMS was detected by Annexin V/APC apoptosis detection kit (**p<0.01, t-test, based on 3 biological replicates). **C** The shMPG was induced in LN-229-C25 shMPG^{IPTG} followed by MMS treatment and the relative growth was determined as in **A** (untreated, grey; IPTG [62.5ng/ml], green; MMS [200nM], red; combination, yellow). **D** Relative cell death (Cytotox, red chanel IncuCyte) in response to MMS treatment was monitored in BS153-C01-HTATIP2^{Dox} over 72h using the same treatment scheme as in **A** and inducing HTATIP2 with Dox [500ng/l]. **E** the relative cell death at 24h was determined with Annexin V/PAC and quantified as in **B**. **F** relative cell death in response to MMS was monitored in BS-153-C01-shMPG^{IPTG} (Cytotox, red channel IncuCyte) over 72h upon depletion of MPG (untreated, grey; IPTG [125ng/ml], green; MMS [200nM], red; combination, yellow).

Supplementary Files

This is a list of supplementary files associated with this preprint. Click to download.

- SupplementAnimation1LN229C25Dox0PDI.mp4
- SupplementAnimation2LN229C25Dox250PDI.mp4
- SupplementFullWesternBlotsFig2ABV2.pdf
- SupplemtaryTablesXFiguresNguyen.pdf